Remote modification of bidentate phosphane ligands controls photonics properties in their complexes: CMe_2 to NR replacement results in enhanced performance of [Cu(RN-xantphos)(N^N)][PF_6] complexes in light-emitting electrochemical cells.

Nina Arnosti, Fabian Brunner, Isidora Susic, Sarah Keller, José M. Junquera-Hernández, Alessandro Prescimone, Henk J. Bolink, Michele Sessolo, Enrique Ortí,* Catherine E. Housecroft* and Edwin C. Constable**

N. Arnosti, F. Brunner, Dr. S. Keller, Dr. A. Prescimone, Prof. C. E. Housecroft, Prof. E. C. Constable
Department of Chemistry
University of Basel
Spitalstrasse 51, CH-4056 Basel, Switzerland
E-mail: catherine.housecroft@unibas.ch; edwin.constable@unibas.ch

I. Susic, Dr. J. M. Junquera-Hernández, Prof. H. J. Bolink, Dr. M. Sessolo, Prof. E. Ortí
Instituto de Ciencia Molecular
Universidad de Valencia
C/ Beltrán 2, 46980 Paterna, Spain.
E-mail: michele.sessolo@uv.es ; enrique.orti@uv.es

Keywords: ionic copper complexes, DFT, photophysics, electroluminescence, light-emitting electrochemical cells

Abstract

A series of copper(I) complexes of the type [Cu(HN-xantphos)(N^N)][PF_6] and [Cu(BnN-xantphos)(N^N)][PF_6], in which N^N = bpy, Mebpy and Me_2bpy, HN-xantphos = 4,6-bis(diphenylphosphanyl)-10H-phenoxazine and BnN-xantphos = 10-benzyl-4,6-bis(diphenylphosphanyl)-10H-phenoxazine is described. The single crystal structures of [Cu(HN-xantphos)(Mebpy)][PF_6] and [Cu(BnN-xantphos)(Me_2bpy)][PF_6] confirm the presence of N^N and P^P chelating ligands with the copper(I) atoms in distorted coordination environments. Solution electrochemical and photophysical properties of the BnN-xantphos-containing compounds (for which the highest-occupied molecular orbital is located on the phenoxazine moiety) are reported. The first oxidation of [Cu(BnN-xantphos)(N^N)][PF_6]

occurs on the BnN-xantphos ligand. Time-dependent density functional theory (TD-DFT) calculations have been used to analyze the solution absorption spectra of the [Cu(BnN-xantphos)(N^N)][PF_6] compounds. In the solid-state, the compounds show photoluminescence in the range 518–555 nm for [Cu(HN-xantphos)(N^N)][PF_6] and 520–575 nm for [Cu(BnN-xantphos)(N^N)][PF_6] with a blue-shift on going from bpy to Mebpy to Me_2bpy. [Cu(BnN-xantphos)(Me_2bpy)][PF_6] exhibits a solid-state photoluminescence quantum yield of 55% with an excited state lifetime of 17.4 μs. Bright light-emitting electrochemical cells were obtained using this complex, and we show that the electroluminescence quantum yield can be enhanced by using less conducting hole injection layers.

1. Introduction

Photoluminescence arising from the metal-to-ligand charge transfer (MLCT) triplet state of copper(I) complexes with 2,2'-bipyridine (bpy) or 1,10-phenanthroline combined with phosphane or bis(phosphane) ligands, $[Cu(P^P)(N^N)]^+$ complexes, was first described by McMillin.[1,2] Current development of technologies for solid-state lighting, and in particular light-emitting electrochemical cells (LECs) based upon solid state electroluminescent materials,[3,4,5] coupled with the use of Earth-abundant metals has led to a growing interest in $[Cu(P^P)(N^N)]^+$ ionic transition-metal complexes (iTMCs), in which the chelating P^P ligand is often bis(2-(diphenylphosphino)phenyl)ether (POP) or 4,5-bis(diphenylphosphino)-9,9-dimethylxanthene (xantphos, Scheme 1). The fact that many compounds in this family exhibit thermally activated delayed fluorescence (TADF), which results in an indirect harvesting of singlet-state fluorescence and a concomitant enhancement in light emission, makes their investigation especially relevant.[6,7,8]

Despite the wide variety of N^N ligands that have been incorporated into [Cu(POP)(N^N)][PF_6] and [Cu(xantphos)(N^N)][PF_6] compounds, some of the most

promising in terms of LEC performance contain simple 6-alkyl, 6-alkyloxy or 6,6'-dialkyl substituted bpy ligands with small alkyl or alkyloxy groups.[9,10,11,12] These iTMCs exhibit fast electroluminescence turn-on times and a LEC containing [Cu(xantphos)(Me_2bpy)][PF_6] (Me_2bpy = 6,6'-dimethyl-2,2'-bipyridine) achieved a maximum efficacy of 3.0 cd A^{-1} (luminance = 145 cd m^{-2}) with a device lifetime of 1 h. We have reported increased lifetimes of >15 h for a LEC with [Cu(xantphos)(Mebpy)][PF_6] but this is at the expense of the efficacy (1.9 cd A^{-1}). LECs containing the iTMCs [Cu(xantphos)(Etbpy)][PF_6] and [Cu(POP)(Etbpy)][PF_6] have achieved device lifetimes of 50 and 80 h, respectively.10 A LEC in which the iTMC was [Cu(POP)(MeObpy)][PF_6] (MeObpy = 6-methoxy-2,2'-bipyridine) was found to be very stable (lifetime >200 h) but was slow to turn-on and had a maximum luminance of only 17 cd m^{-2}.11 The trade-off between brightness and device lifetime, not only in copper-based but also in iridium-based LECs, is something that we and others regularly encounter10,13,14 and is a major hurdle to the practical application of these devices.

The typical choices of P^P ligands in [Cu(P^P)(N^N)]$^+$ iTMCs for LEC applications are POP and xantphos, and the presence of the aryl substituents on the phosphorus atoms appears crucial for superior photophysical properties. We have demonstrated that replacing the PPh_2 groups in xantphos by P^tBu_2 units leads to weak emissions, both in solution and the solid state, probably due to vibrational quenching effects.[15] The HN-xantphos ligand, in which the CMe_2 group of the xanthene backbone is replaced by NH, is, like POP and xantphos, commercially available and has been extensively used as a wide bite-angle bis(phosphane) in homogeneous catalysis.[16,17,18,19,20] [Cu(HN-xantphos)(Me_2Ph_2phen)][PF_6] (Me_2Ph_2phen = 2,9-dimethyl-4,7-diphenyl-1,10-phenanthroline) was reported by Beller and coworkers[21] as a member of a series of [Cu(P^P)(Me_2Ph_2phen)]$^+$ complexes used as photosensitizers in the photocatalytic H_2 generation from water under basic conditions. [Cu(HN-xantphos)(ppipH)][ClO_4] (ppipH = 2-(pentafluo-rophenyl)-1H-imidazo[4,5-f][1,10]-phenanthroline) has been reported and exhibits an emission maximum at 570 nm in the solid

state (λ_{exc} = 365 nm), although no photoluminescence quantum yield was given [X. Liu, Y. Shan, J. Xu, X. Zhang, S. Shang, X-L. Li, *Polyhedron*, 2019, **164**, 152–158.]. However, there appear to be no examples in the literature of [Cu(RN-xantphos)(N^N)]$^+$ iTMCs used in LECs.

We here report the synthesis and characterization of [Cu(HN-xantphos)(N^N)][PF_6] and [Cu(BnN-xantphos)(N^N)][PF_6] complexes, in which HN-xantphos and BnN-xantphos bear an NH and NCH_2Ph functionality, respectively and the N^N ligands are bpy, 6-methyl-2,2'-bipyridine (Mebpy) and 6,6'-dimethyl-2,2'-bipyridine (Me_2bpy). The effects of substituting the widely used xantphos P^P ligand by HN-xantphos and BnN-xantphos on both the photophysical properties of the compounds and the application in LECs of the most emissive one are described.

2. Results and discussion

2.1. Synthesis and solution characterization of copper(I) complexes

The P^P ligand BnN-xantphos (**Scheme 1**) was prepared by the reaction of HN-xantphos with benzyl chloride as previously reported.16 [Cu(HN-xantphos)(N^N)][PF_6] and [Cu(BnN-xantphos)(N^N)][PF_6] with N^N = bpy, Mebpy and Me_2bpy (Scheme 1) were synthesized by adding a CH_2Cl_2 solution of the P^P and N^N ligands to a CH_2Cl_2 solution of [$Cu(MeCN)_4$][PF_6]. After work up, the [Cu(HN-xantphos)(N^N)][PF_6] compounds were isolated as pale, greenish-yellow solids in 50.7–98.7% yields, whereas the pale yellow [Cu(BnN-xantphos)(N^N)][PF_6] complexes were obtained in 71.5–88.5% yields. The electrospray mass spectrum of each compound showed two dominant peak envelopes (Figures S1–S6) arising from the [M–PF_6]$^+$ and [M–PF_6–(N^N)]$^+$ ions. Isotope distributions were consistent with those expected.

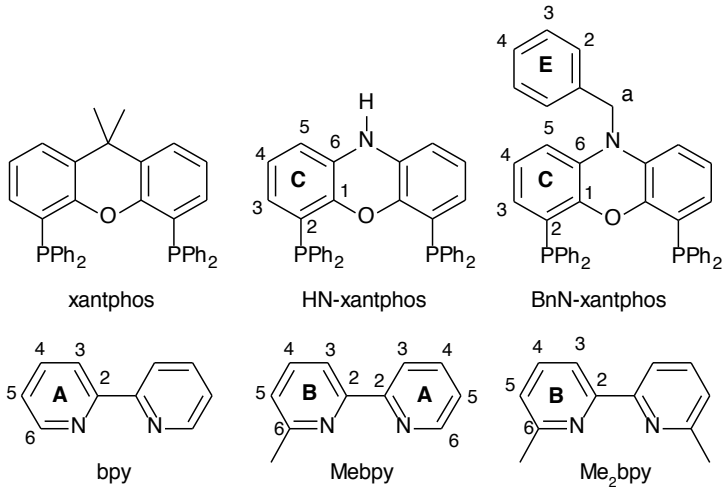

Scheme 1. Structures of xantphos and the ligands employed in this work. Atom labels for NMR spectroscopic assignments are shown; the phenyl rings in the PPh_2 groups of POP and xantphos are labelled D.

^{1}H and $^{13}C\{^{1}H\}$ NMR spectra were recorded in acetone-d_6 for the series of compounds containing HN-xantphos and in CD_2Cl_2 for the [Cu(BnN-xantphos)(N^N)][PF_6] complexes. The benzyl-substituted compounds were not sufficiently soluble in acetone-d_6 to record NMR spectra, whereas the [Cu(HN-xantphos)(N^N)][PF_6] complexes were unstable with respect to the formation of homoleptic [$Cu(N^N)_2$][PF_6] in CD_2Cl_2. Assignments of the ^{1}H and $^{13}C\{^{1}H\}$ NMR spectra were made using COSY, NOESY, HMQC and HMBC methods, and ring and atom labelling for the ligands are displayed in Scheme 1. **Figure 1** compares the high-frequency regions of the ^{1}H NMR spectra of the HN-xantphos-containing compounds (see Figure S7 in the Supporting Information for the BnN-xantphos compounds).

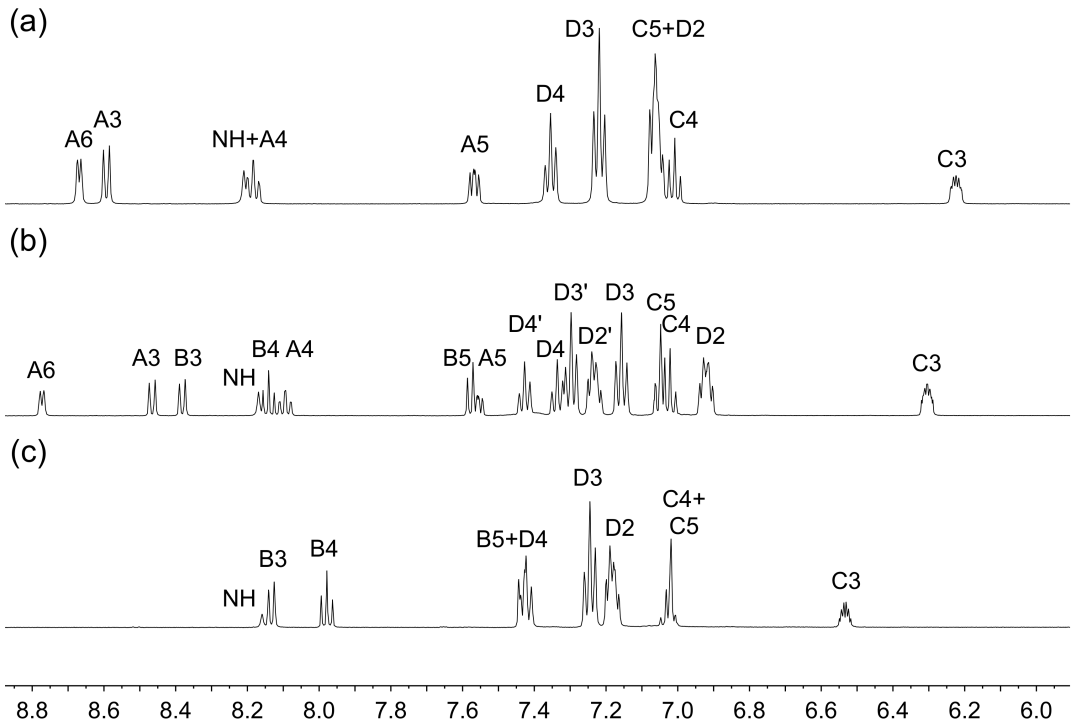

Figure 1. High-frequency regions of the solution ^{1}H NMR spectra (500 MHz, acetone-d_6, 298 K) for (a) [Cu(HN-xantphos)(bpy)][PF_6], (b) [Cu(HN-xantphos)(Mebpy)][PF_6] and (c) [Cu(HN-xantphos)(Me_2bpy)][PF_6].

The signal for the NH proton appears at δ 8.21, 8.17 and 8.16 ppm in [Cu(HN-xantphos)(bpy)][PF_6], [Cu(HN-xantphos)(Mebpy)][PF_6] and [Cu(HN-xantphos)(Me_2bpy)][PF_6], respectively. Differences in the signals for the A and B rings in Figure 1a-c are consistent with the introduction of methyl groups in the 6-position (Figure 1b) and 6,6'-positions (Figure 1c) of the bpy ligand. In Figures 1a and 1c, the appearance of one set of signals (H^{D2}, H^{D3} and H^{D4}) for the P-attached phenyl rings is consistent with the presence of a symmetrical bpy or Me_2bpy ligand. For the asymmetrical Mebpy, the D rings split into two sets: those pointing up (labelled D), which give rise to a NOESY cross-peak between protons H^{D2} and $H^{Me(ring\ B)}$, and those pointing down (labelled D'), which give a NOESY cross-peak between protons $H^{D2'}$ and H^{A6}. This is better appreciated with reference to the structural discussion which follows.

2.2. Crystal structures

Single crystals of [Cu(HN-xantphos)(Mebpy)][PF_6]·0.5CH_2Cl_2 and [Cu(BnN-xantphos)(Me_2bpy)][PF_6]·CH_2Cl_2 were grown by diffusion of Et_2O into CH_2Cl_2 solutions of the compounds. The compounds crystallize in the orthorhombic space groups *Aba*2 and *Pbca*, respectively. The structures of the two complex cations are shown in **Figure 2**a and **2**b, with selected bond distances and angles listed in the figure caption. Each copper(I) center is in a distorted tetrahedral environment, with P–Cu–P chelate angles of the HN-xantphos and BnN-xantphos ligands of 120.67(3) and 118.87(3)°, respectively. These values compare to the calculated natural bite angles (defined only by the constraints of the ligand backbone) of 114.2 and 114.1°, respectively.[22]

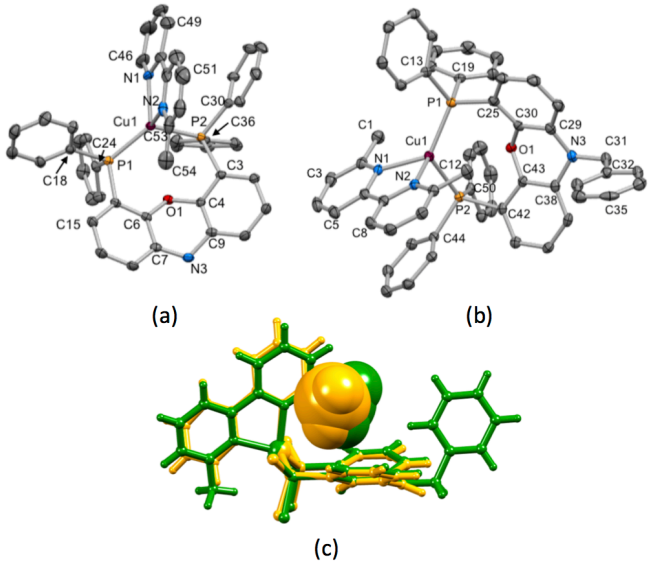

Figure 2. (a) Structure (ellipsoids at 40% probability level and H atoms omitted) of the [Cu(HN-xantphos)(Mebpy)]$^+$ cation. Selected bond parameters: Cu1–P1 = 2.2344(9), Cu1–P2 = 2.2925(9), Cu1–N1 = 2.080(3), Cu1–N2 = 2.067(3) Å; P1–Cu1–P2 = 120.67(3), P1–Cu1–N1 = 124.95(10), P2–Cu1–N1 = 99.62(9), P1–Cu1–N2 = 120.32(9), P2–Cu1–N2 = 103.01(9), N1–Cu1–N2 = 79.56(15)°. (b) Structure (ellipsoids at 40% probability level and H atoms omitted) of the [Cu(BnN-xantphos)(Me_2bpy)]$^+$ cation. Selected bond parameters: Cu1–P2 = 2.3088(9), Cu1–P1 = 2.2508(9), Cu1–N2 = 2.088(3), Cu1–N1 = 2.106(3) Å; P1–Cu1–P2 = 118.87(3), N2–Cu1–P2 = 102.70(7), N2–Cu1–P1 = 119.84(7), N2–Cu1–N1 = 79.84(10), N1–Cu1–P2 = 99.57(7), N1–Cu1–P1 = 127.80(8)°. (c) Overlay of the structures of the [Cu(HN-

xantphos)(Mebpy)]$^+$ (orange) and [Cu(BnN-xantphos)(Me$_2$bpy)]$^+$ (green) cations. For clarity, only the *ipso*-C atoms of the P-bonded phenyl rings are shown. The Me groups lying over the phenoxazine 'bowl' (lower right) are depicted in space-filling representation.

The conformation of the phenoxazine unit is virtually identical in the two structures as the overlay in Figure 2c shows. The central ring adopts a boat conformation (Figure 2c and S8a†) leading to the phenoxazine unit presenting a 'bowl'-like unit. The sum of the C–N–C bond angles around atom N3 in [Cu(BnN-xantphos)(Me$_2$bpy)]$^+$ is 353.6(5)°, indicative of an sp^2 hybridization. Differences between the corresponding C–N bond distances (N3–C38 = 1.414(4), N3–C29 = 1.406(4), N3–C31 = 1.452(4) Å) imply π-contributions to C29–N3 and C38–N3. In the [Cu(HN-xantphos)(Mebpy)]$^+$ cation, the Mebpy ligand is oriented with the 6-methyl group lying over the phenoxazine 'bowl', and one of the methyl groups in [Cu(BnN-xantphos)(Me$_2$bpy)]$^+$ is similarly positioned (Figure 2c). We have previously commented upon comparable orientational preferences of asymmetrical 6-substituted bpy ligands in [Cu(xantphos)(6-Rbpy)]$^+$ cations.[10,11,23]

The bpy unit in both structures is close to planar with the angle between the least squares planes of the two pyridine rings being 7.6° in [Cu(HN-xantphos)(Mebpy)]$^+$ and 5.8° in [Cu(BnN-xantphos)(Me$_2$bpy)]$^+$. Each bpy unit engages in a π-stacking interaction with one of the P-bonded phenyl rings (Figure 2b). In [Cu(HN-xantphos)(Mebpy)]$^+$, the angle between the least squares planes through the phenyl ring containing C30 and the bpy unit is 14.0°, and the distance between the centroids of the rings with C30 and N1 is 3.93 Å (and with N2 = 4.26 Å). In [Cu(BnN-xantphos)(Me$_2$bpy)]$^+$, the angle between the planes through the bpy unit and the phenyl ring containing C44 is 13.3°, and the distance between the centroids of the rings containing C44 and N1 is 3.82 Å (4.40 Å for the ring with N2). Although the benzyl arene ring in [Cu(BnN-xantphos)(Me$_2$bpy)][PF$_6$] is not involved in either intra- or

intermolecular face-to-face π-stacking contacts, it exhibits an intermolecular π–CH[24] contact (centroid...H3^{i}C3^{i} = 2.75 Å, symmetry code i = 1–*x*, $^{1}/_{2}$+*y*, $^{3}/_{2}$–*z*).

2.3. DFT calculations

The geometries of the [Cu(HN-xantphos)(N^N)]$^{+}$ and [Cu(BnN-xantphos)(N^N)]$^{+}$ complexes in the ground electronic state (S_0) were optimized at the DFT B3LYP-3D/(def2svp+def2tzvp) level. Calculations reproduce the main features discussed above for the X-ray geometries of [Cu(HN-xantphos)(Mebpy)]$^{+}$ and [Cu(BnN-xantphos)(Me$_2$bpy)]$^{+}$: 1) the atoms forming the coordination sphere of the Cu atom define a distorted tetrahedral structure, 2) the phenoxazine unit adopts a 'bowl'-like conformation in which the 6-methyl substituent of the complexes with Mebpy ligands lies, 3) the bpy ligands are quasi-planar with twist angles less than 10°, 4) the face-to-face π-stacking interaction between one of the phenyl rings of the PPh$_2$ units and the bpy ligand, 5) the π-character of the C–N bonds of the phenoxazine unit with bond lengths of 1.40–1.41 Å, and 6) the orthogonal disposition of the benzyl ring with respect to the phenoxazine moiety in the [Cu(BnN-xantphos)(N^N)]$^{+}$ complexes with a C–H···N distance of 2.52 Å. Figure S9 shows the minimum-energy structures calculated for [Cu(HN-xantphos)(Me$_2$bpy)]$^{+}$ and [Cu(BnN-xantphos)(Me$_2$bpy)]$^{+}$ as representative examples.

The frontier molecular orbitals calculated for the [Cu(HN-xantphos)(N^N)]$^{+}$ and [Cu(BnN-xantphos)(N^N)]$^{+}$ complexes are shown in **Figure 3**, together with those computed for [Cu(xantphos)(bpy)]$^{+}$ included as a reference for comparison purposes. The lowest-unoccupied molecular orbital (LUMO) is located over the bpy ligand exhibiting an identical atomic orbital composition for all the complexes. It has a rather similar energy (–2.56 eV) for [Cu(xantphos)(bpy)]$^{+}$, [Cu(HN-xantphos)(N^N)]$^{+}$ and [Cu(BnN-xantphos)(N^N)]$^{+}$, and undergoes a gradual destabilization upon addition of electron-donating Me substituents to the bpy ligand (Figure 3). This effect was already observed for similar series of Cu

complexes.[25,26] Therefore, more negative reduction potentials are expected along both series of complexes. Regarding the highest-occupied molecular orbital (HOMO), it is calculated at –6.00 eV for $[Cu(xantphos)(bpy)]^+$ and mainly resides over the metal atom with some extension to the neighboring phosphorus atoms (Figure 3). An MO featuring an identical topology and appearing at almost the same energy is found for the HN-xantphos- and BnN-xantphos-containing complexes, but it now corresponds to the HOMO–1. For these complexes, the HOMO is calculated at higher energies around –5.75 eV and is placed over the phenoxazine unit. This MO also exists for the reference $[Cu(xantphos)(bpy)]^+$ complex but it is calculated 1 eV lower in energy (–6.76 eV) and corresponds to the HOMO–3.

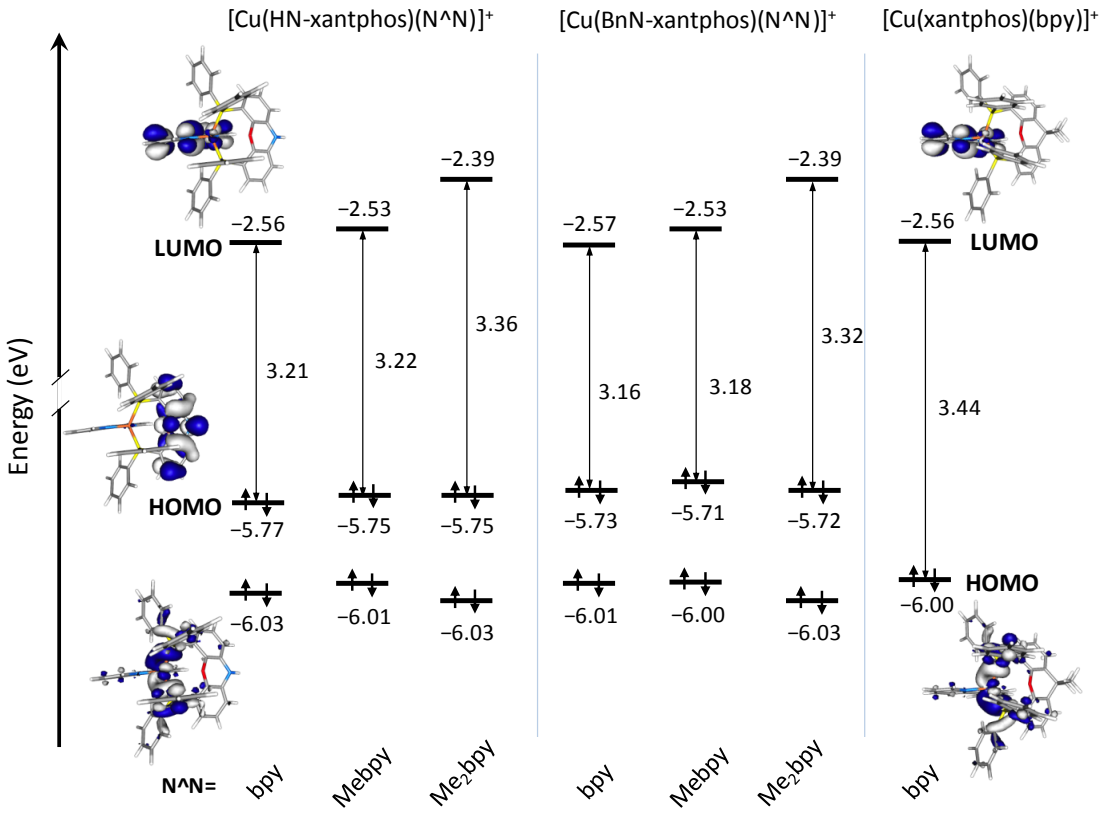

Figure 3. Energy diagram displaying the energies calculated for the frontier molecular orbitals of $[Cu(HN\text{-}xantphos)(N^N)]^+$, $[Cu(BnN\text{-}xantphos)(N^N)]^+$ and $[Cu(xantphos)(bpy)]^+$ complexes. The HOMO–LUMO energy gaps are also quoted. Isovalue contour plots (±0.03 a.u.) are shown for MOs of complexes $[Cu(HN\text{-}xantphos)(bpy)]^+$ and $[Cu(xantphos)(bpy)]^+$. The topology calculated for the corresponding MOs of the other complexes is similar.

The presence of the π-conjugated nitrogen atom in the RN-xantphos-type ligands (R = H or Bn) instead of the CMe_2 unit present in the xantphos ligand destabilizes the MO and places it as the HOMO at almost constant energies around 0.25 eV above the HOMO–1 centered on the metal and the phosphorus atoms. As discussed below, this has special consequences on the oxidation behavior of the $[Cu(HN\text{-}xantphos)(N\text{^}N)]^+$ and $[Cu(BnN\text{-}xantphos)(N\text{^}N)]^+$ complexes, for which less positive oxidation potentials have to be expected compared to xantphos-containing complexes. Since both the HOMO and the HOMO–1 remain almost constant in energy for the $[Cu(HN\text{-}xantphos)(N\text{^}N)]^+$ and $[Cu(BnN\text{-}xantphos)(N\text{^}N)]^+$ complexes, the HOMO−LUMO and also the (HOMO–1)−LUMO energy gap gradually widens along each series of complexes as the number of Me substituents increases. Therefore, it is expected that the first triplet excited state (T_1) features increasing energies along the series, leading to blue-shifted light emission as Me groups are added. This is consistent with the description of the first triplet state previously discussed for complexes bearing the xantphos ligand.[10,25,26,27]

2.4. Electrochemistry and oxidized species

The instability of the $[Cu(HN\text{-}xantphos)(N\text{^}N)][PF_6]$ compounds in CH_2Cl_2 (see above) precluded the electrochemical investigation of these compounds in CH_2Cl_2. Attempts to find another suitable solvent were unsuccessful, largely due to solubility issues. Therefore, we decided to focus only on the $[Cu(BnN\text{-}xantphos)(N\text{^}N)][PF_6]$ complexes. The electrochemical properties of the BnN-xantphos ligand and of the copper(I) complexes were investigated by cyclic voltammetry in CH_2Cl_2, and the redox processes are summarized in **Table 1**. Figure S10 shows the cyclic voltammograms (CVs) recorded for BnN-xantphos and $[Cu(BnN\text{-}xantphos)(N\text{^}N)][PF_6]$ (N^N = bpy, Mebpy, Me_2bpy). The BnN-xantphos ligand shows a quasi-reversible oxidation process at +0.33 V, which was assigned to oxidation of the

electron-rich BnN environment. No reduction processes were observed within the solvent accessible window. The CV of each copper(I) complex (Figure S10) exhibits a single oxidation process. In good agreement with the theoretical predictions, the $E_{1/2}^{ox}$ values of +0.58, +0.62 and +0.61 V recorded for the BnN-xantphos-containing complexes (Table 1) are significantly lower than the values of +0.76, +0.85 and +0.90 V previously reported for the xantphos complexes [Cu(xantphos)(bpy)][PF_6], [Cu(xantphos)(Mebpy)][PF_6] and [Cu(xantphos)(Me_2bpy)][PF_6], respectively.[26] As discussed above, in the xantphos complexes the HOMO is located on the copper atom and its phosphorus environment and the oxidation process mainly arises from a Cu^+/Cu^{2+} process. In contrast, for the BnN-xantphos-containing compounds, the HOMO fully resides on the phenoxazine moiety at higher energies (Figure 3) and the first oxidation is expected to be ligand-centered. Taking the scan past +1.0 V leads to the observation of a second (irreversible) oxidative process, assigned to a phosphane oxidation.

Table 1. Cyclic voltammetry data for [Cu(BnN-xantphos)(N^N)][PF_6] complexes in CH_2Cl_2 (ca. 2×10^{-3} M, vs. Fc^+/Fc, [$^nBu_4N$][PF_6] as supporting electrolyte, scan rate = 0.1 V s^{-1}).

Compound	Oxidation	Reduction
	$E_{1/2}^{ox}$ / V (E_{pc}–E_{pa} /mV)	E_{pa}^{red} / V
BnN-xantphos	+0.33 (100)	-
[Cu(BnN-xantphos)(bpy)][PF_6]	+0.58 (110)	-2.15
[Cu(BnN-xantphos)(Mebpy)][PF_6]	+0.62 (120)	-2.20
[Cu(BnN-xantphos)(Me_2bpy)][PF_6]	+0.61 (110)	-2.23

All the complexes show an irreversible reduction process (Table 1 and Figure S10) which moves to more negative potentials on going from bpy to Mebpy to Me_2bpy. This trend was previously observed in series of related complexes,27 and is consistent with the LUMO being located on the N^N ligand and increasing in energy with the number of Me groups (Figure 3). To investigate in more detail the oxidation processes, the dication and trication species of the

[Cu(HN-xantphos)(bpy)]$^+$ and [Cu(BnN-xantphos)(bpy)]$^+$ were calculated theoretically. In both cases, the oxidation of the cation leading to the 2+ species takes place over the phenoxazine unit. This is clearly reflected by the electron spin-density plots computed for the dication species, which show that the unpaired electron resides over the RN-xantphos (R = H or Bn) region, reproducing the topology of the HOMO (Figure S11). After extracting the first electron, the electron density of the molecules rearranges and both the α and β HOMOs of the open-shell dication are located on the copper atom and its phosphorus environment (Figure S12), and the extraction of the second electron to produce the 3+ species takes place from this part of the molecule. The spin-density plots calculated for the optimized trications clearly show that one unpaired electron resides over the phenoxazine moiety and the other spans over the CuP_2 environment (Figure S11). The trications are therefore calculated as open-shell triplet species.

2.5. Photophysical behavior

The solution absorption spectra of the [Cu(BnN-xantphos)(N^N)][PF_6] compounds (**Figure 4**a and **Table 2**) are dominated by intense bands below 350 nm arising from spin-allowed $\pi\rightarrow\pi^*$ and $n\rightarrow\pi^*$ transitions. The shift to lower energies of the shoulder around 307–319 nm as additional methyl groups are introduced into the bpy unit is also a feature of the analogous [Cu(xantphos)(N^N)][PF_6] compounds.[10] The low intensity absorption band at around 400 nm in Figure 4a most likely arises from transitions to metal-to-ligand charge transfer (MLCT) excited states. Figure 4a also shows the absorption spectrum of [Cu(xantphos)(Me_2bpy)][PF_6] in which the MLCT band is clearly visible. Because of the instability of the [Cu(HN-xantphos)(N^N)][PF_6] compounds in CH_2Cl_2 (see earlier), reliable solution absorption spectra could not be obtained for these complexes. Although the compounds are stable with respect to ligand redistribution in acetone, the UV-Vis cut-off of 330 nm rendered this an unsuitable alternative solvent. The theoretical absorption spectrum of complex [Cu(BnN-

xantphos)(bpy)]$^+$ was simulated (Figure S13) by calculating the first 300 singlet excited states at the optimized geometry of S_0 using the time-dependent DFT (TD-DFT) approach. As in the experimental spectrum (Figure 4a), the most intense absorption band appears below 300 nm and originates from a manifold of transitions of both π→π* and *n*→π* nature. Above 325 nm, two bands are predicted, both corresponding to excited states of MLCT nature. The lowest-energy band computed at 442 nm is correlated with the experimental band observed at 400 nm and is mainly due to the HOMO–1→LUMO excitation (87%) associated to an electron promotion from the CuP_2 environment to the bpy ligand (Figure 3). The HOMO→LUMO excitation involving a ligand-to-ligand charge transfer (LLCT) from the phenoxazine moiety to the bpy ligand is actually calculated at lower energies (460 nm) but it shows a negligible intensity with an oscillator strength (*f*) of only 0.002. This is the reason why the lowest-energy band observed in the experimental UV-Vis spectra appears at similar wavelengths (~ 400 nm) for both BnN-xantphos- and xantphos-containing complexes (Figure 4a). The band observed around 335−340 nm is associated to the band calculated at 346 nm for [Cu(BnN-xantphos)(bpy)]$^+$ and results from the HOMO–1→LUMO+1 (95%) MLCT excitation. Solution emission spectra were recorded for the [Cu(BnN-xantphos)(N^N)][PF_6] complexes, exciting into the MLCT band (λ_{exc} = 410 nm) (Table 2 and Figure S14). The solution emissions are weak, but show a blue-shift from 650 to 600 to 560 nm upon introducing one, then two Me groups into the bpy unit. This trend follows those previously observed for related [Cu(P^P)(N^N)][PF_6] series.27 Photoluminescence quantum yields (PLQYs) measured in deaerated solutions are lower than 2% and the compounds exhibit very short excited-state lifetimes (Table 2).

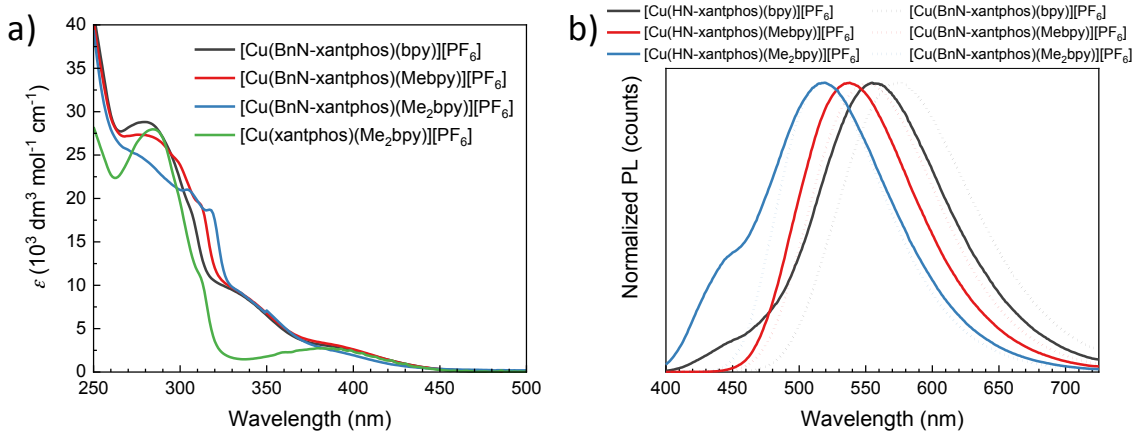

Figure 4. a) Absorption spectra of solutions (2.5×10^{-5} M in CH_2Cl_2) of [Cu(BnN-xantphos)N^N)][PF_6] with N^N = bpy, Mebpy and Me_2bpy compared with the spectrum of [Cu(xantphos)(Me_2bpy)][PF_6]. b) Photoluminescence spectra of powder samples of [Cu(HN-xantphos)(N^N)][PF_6] and [Cu(BnN-xantphos)N^N)][PF_6] with N^N = bpy, Mebpy and Me_2bpy (λ_{exc} = 375 nm).

Solid-state emission data were recorded for all the [Cu(HN-xantphos)(N^N)][PF_6] and [Cu(BnN-xantphos)(N^N)][PF_6] compounds (Table 2 and Figure 4b). For each series of compounds, the emission maximum blue-shifts on going from bpy to Mebpy to Me_2bpy consistent with earlier reports,27 whereas the attachment of the benzyl group to the phenoxazine moiety of the P^P ligand causes a red-shift ranging from 20 nm for [Cu(P^P)(bpy)][PF_6] to 2 nm for [Cu(P^P)(Me_2bpy)][PF_6]. As expected from our previous investigations of [Cu(xantphos)(N^N][PF_6] complexes,9,10,27 the presence of 6-methyl or 6,6'-dimethyl substituents in the bpy domain is beneficial in terms of PLQY and excited-state lifetime (Table 2).

Table 2. Photophysical characterization for deaerated solutions (CH_2Cl_2, 2.5×10^{-5} M) and powder of the [Cu(N^N)(P^P)][PF_6] complexes.

Compound	Solution				Powder		
	λ_{max}^{abs} (nm) (ε_{max}, $dm^3\ mol^{-1}\ cm^{-1}$)	λ_{max}^{em} (nm)[a]	PLQY (%)	τ (μs)	λ_{max}^{em} (nm)[b]	PLQY (%)	τ (μs)
[Cu(HN-xantphos)(bpy)][PF_6]	-	-	-	-	555	5	1.77
[Cu(HN-xantphos)(Mebpy)][PF_6]	-	-	-	-	535	17	10.8
[Cu(HN-xantphos)(Me_2bpy)][PF_6]	-	-	-	-	518	14	14.2
[Cu(BnN-xantphos)(bpy)][PF_6]	280 (28,800), 307 sh (18,200), 335 sh (9,200), 400 (2,600)	650	1	0.03	575	2	1.8
[Cu(BnN-xantphos)(Mebpy)][PF_6]	285 (27,000), 313 sh (18,800), 338 sh (8,700), 396 (2,800)	600	1	0.24	550	8	7.5
[Cu(BnN-xantphos)(Me_2bpy)][PF_6]	281 (24,300), 306 sh (20,800), 319 sh (18,200), 341 sh (8,200), 402 (1,800)	560	1	0.47	520	55	17.4

(a) $\lambda_{exc} =$ 410 nm; (b) $\lambda_{exc} =$ 375 nm.

The electronic nature of the emitting triplet states of the copper(I) complexes studied was investigated using TD-DFT calculations. Table S1 summarizes the vertical excitation energies and electronic description calculated for the first three triplet states (T_1 to T_3) and the lowest-energy singlet excited state (S_1). The results obtained for the reference [Cu(xantphos)(bpy)]$^+$ complex are included for comparison purposes. The T_1 triplet corresponds, in all the complexes, to a state of MLCT nature involving an excitation from an MO centered on the metal atom (the HOMO in the reference complex, the HOMO–1 in HN-xantphos and BnN-xantphos complexes) to the LUMO centered on the bpy-moiety. The T_1 state is calculated at the same energy (~2.55 eV) for the [Cu(xantphos)(bpy)]$^+$, [Cu(HN-xantphos)(bpy)]$^+$ and Cu(BnN-xantphos)(bpy)]$^+$ complexes and increases in energy as Me groups are added to the bpy ligand. This is agreement with the destabilization of the LUMO induced by the addition of Me substituents discussed above (Figure 3). As the energy difference between T_1 and T_2 is relevant (0.15−0.20 eV), it is therefore expected that the phosphorescent emission takes place

from T_1 and shifts to shorter wavelengths along each series in good agreement with the experimental data (Table 2).

To further investigate the electronic nature of the emitting state, the geometry of the lowest-energy triplet of each complex was optimized at the unrestricted UDFT level. The electron-unpaired spin-density plots calculated for the optimized T_1 state of $[Cu(xantphos)(bpy)]^+$ and $Cu(HN\text{-}xantphos)(bpy)]^+$ are displayed in Figure 5 as representative examples.

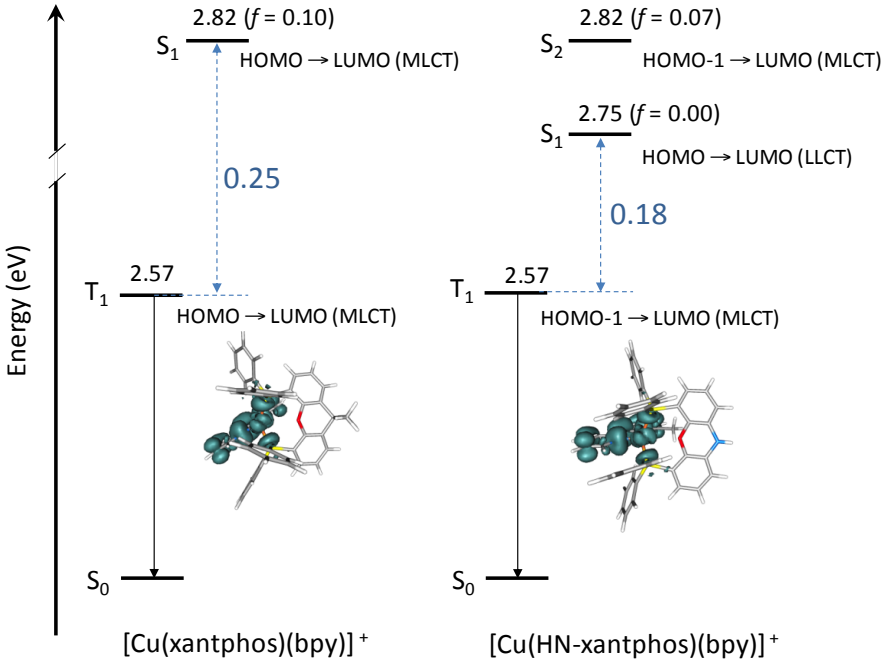

Figure 5. Energy diagram of the lowest-energy excited states calculated at the TD-DFT level for $[Cu(xantphos)(bpy)]^+$ and $[Cu(HN\text{-}xantphos)(bpy)]^+$ at the minimum-energy geometry of the ground state S_0. The vertical excitation energy, the main contributing excitation and the nature are indicated for each state. The unpaired-electron spin-density plots (isocontours of 0.002 a.u.) computed at the UDFT level for the fully relaxed T1 state of both complexes are also shown.

These plots show that, in agreement with the TD-DFT predictions, the T_1 state of all the complexes implies a charge transfer from the metal center to the bpy ligand and has an MLCT

nature consistent with the HOMO–1→LUMO excitation (HOMO→LUMO for [Cu(xantphos)(bpy)]$^+$). Therefore, on the basis of both TD-DFT and UDFT calculations, the ^{3}LLCT (HOMO→LUMO) triplet state does not play any special role in the phosphorescent emission of HN-xantphos- and BnN-xantphos complexes. It is also worth mentioning that, as previously discussed for xantphos-containing complexes,[27,25] the partial oxidation of the copper atom in the T_1 state leads to the geometry of the complex in T_1 deviating from the tetrahedral geometry obtained for S_0 and rather tends to adopt a square-planar coordination geometry. This geometrical relaxation is partially restricted by the presence of Me substituents in the 6 and 6'-positions of the bpy ligand,[25,27] and the emission from T_1 blue-shifts upon increasing the number of Me groups.

The occurrence of TADF processes has been previously postulated for Cu(I) complexes with chemical structures similar to those of the complexes studied in this work.[6,7,8] A requirement for TADF is that the energy difference between the lowest-lying T_1 triplet and the emitting singlet excited state S_1 has to be small to favor the reverse inter-system crossing (RISC) from T_1 to S_1. For the [Cu(HN-xantphos)(N^N)]$^+$ and [Cu(BnN-xantphos)(N^N)]$^+$ complexes, the energy difference between S_1 and T_1 is predicted in the range 0.14–0.20 eV at the optimized geometry of S_0 (Table S1), which is lower than that computed for the [Cu(xantphos)(bpy)]$^+$ complex (0.25 eV) and small enough to favor the RISC process (Figure 5). However, the HOMO→LUMO S_1 state in HN-xantphos and BnN-xantphos complexes presents a very small oscillator strength (< 0.01, Table S1), well below that of [Cu(xantphos)(bpy)]$^+$ (f = 0.10), and, if TADF does occur, it will make only a small contribution to the emission. Thus, the RISC process in these complexes would in principle work as a non-radiative decay route instead of increasing the emission through TADF, as it favors the depopulation of the emitting T_1 state to populate a non-emitting singlet excited state.

3. Light-emitting electrochemical cells

In view of the high PLQY (55%) of the [Cu(BnN-xantphos)(Me_2bpy)][PF_6] complex in the solid state, we selected this compound to study its electroluminescence (EL) properties when used as the active layer in LECs. Details of the device fabrication are given in the Supporting Information. LECs are normally deposited on a transparent conducting substrate (glass with indium tin oxide, ITO), coated with poly-(3,4-ethylenedioxythiophene)-poly(styrenesulfonate) (PEDOT:PSS), which is used to smooth the electrode surface and to enlarge its work function (WF). PEDOT:PSS is commercially available in different formulations, with variable WF and conductivity. The two parameters are mutually related and determined by the effective PEDOT to PSS ratio in the formulation.[28] The most common PEDOT:PSS used in LECs (commercial name CLEVIOS™ P VP AI 4083) has a PEDOT to PSS weight ratio of 1:6, exhibiting a conductivity of approximately 10^{-3}-10^{-4} S cm^{-1} and a WF = 4.85 eV. Increasing the amount of PSS in the formulation inevitably results in a lower conductivity, but interestingly it has been shown to enlarge the PEDOT:PSS film WF. PEDOT:PSS films with a PEDOT to PSS ratio of 1:20 (commercially available as CLEVIOS™ P VP CH 8000) have one order of magnitude lower conductivity and WF = 5.2 eV. The latter property is of interest in the design of electroluminescent devices, where a larger WF can facilitate the hole injection from the anode to the adjacent transport or emissive layers. At the same time, the lower conductivity might decrease the non-radiative recombination at the PEDOT:PSS interface, which might be especially important in LECs, as no selective transport layers are used. Hence, here we prepared LECs using either CLEVIOS™ P VP AI 4083 (high conductivity, low WF) or CLEVIOS™ P VP CH 8000 (low conductivity, high WF) as the hole injection layer (HIL).

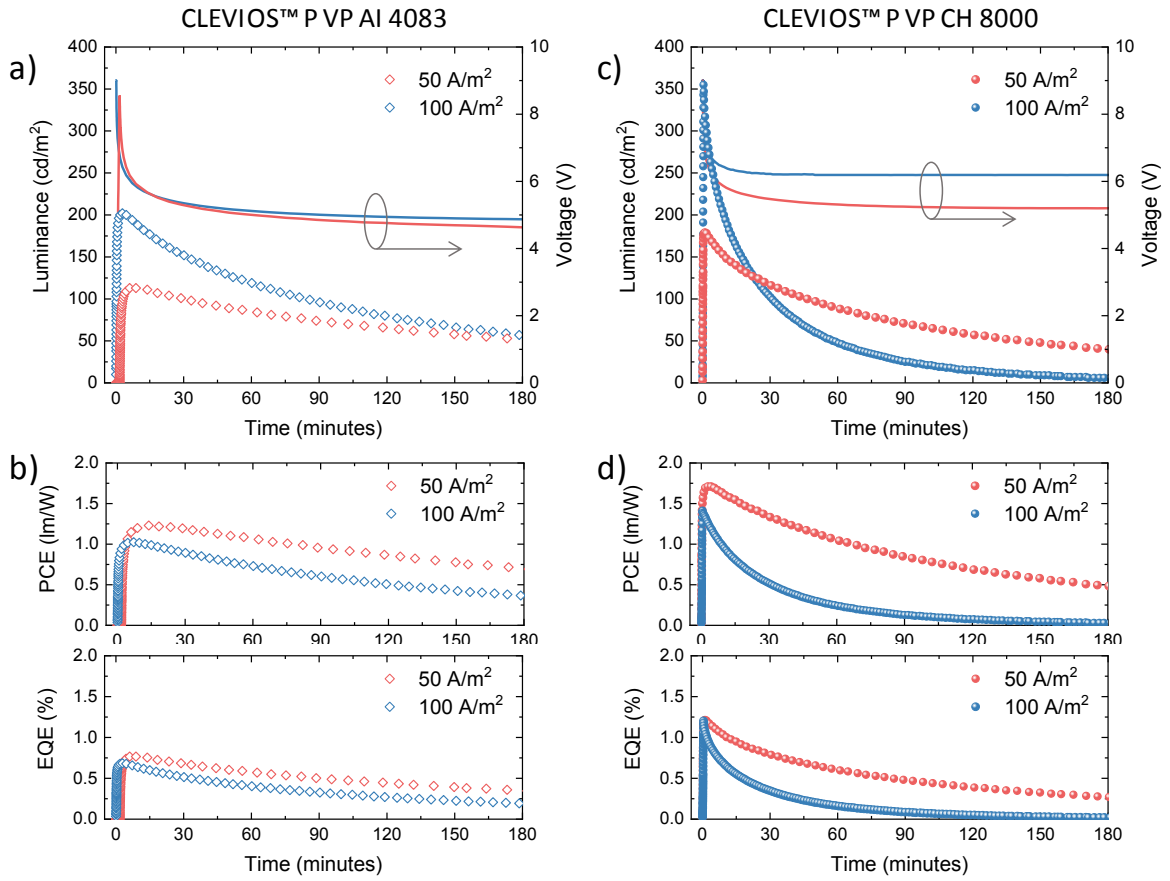

Figure 6. (a, c) Luminance (symbols), voltage (lines) and (b, d) corresponding power conversion efficiency (PCE) and external quantum efficiency (EQE) vs. time for LECs employing CLEVIOS™ P VP AI 4083 (left) or CLEVIOS™ P VP CH 8000 (right) as the hole injection layer.

[Cu(BnN-xantphos)(Me_2bpy)][PF_6] thin films were spin-coated on the different HILs from dichloromethane solution in the presence of the ionic liquid 1-ethyl-3-methylimidazolium hexafluorophosphate, [EMIM][PF_6], in a 4:1 molar ratio. The 100 nm thick films were annealed in a nitrogen-filled glove box prior to the thermal evaporation of an aluminum cathode. LECs were tested without encapsulation in inert atmosphere, applying a pulsed current (50 or 100 A m^{-2} average current density, 1 kHz, 50% duty cycle) and monitoring the voltage and the electroluminescent intensity over time. The optoelectronic characterization is reported in **Figure 6** and the derived device parameters are summarized in **Table 3**. LECs using the CLEVIOS™ P VP AI 4083 as the HIL show fast turn-on times (t_{on},

time to reach 100 cd m^{-2}) of only 12 s when biased at 100 A m^{-2}, and slightly larger at lower current density, approximately 3 minutes (Figure 6a). The peak luminance is proportional to the current density, reaching a maximum of 113 and 203 cd m^{-2} for LECs biased at 50 and 100 A m^{-2}, respectively. The corresponding maximum efficacies (η_{max}) are hence rather similar, 2.26 cd A^{-1} at 50 A m^{-2} and 2.03 cd A^{-1} at 100 A m^{-2}. The lifetimes ($t_{1/2}$, time to reach half of the maximum luminance) are of 155 and 65 minutes for the LECs biased at 50 and 100 A m^{-2}, respectively. Besides the fastest electroluminescence intensity drop for the LECs driven at high current density, all devices exhibit luminance exceeding 50 cd m^{-2} after 3 hours of continuous operation.

Table 3. Device parameters for the set of LECs presented in Figure 3.

HIL	J (A/m^2)	t_{ON} (s)[a]	L_{max} (cd/m^2)	η_{max} (cd/A)	$t_{1/2}$ (min)	PCE_{max} (lm/W)	EQE_{max} (%)
CLEVIOS™ P VP AI 4083	50	185	113	2.26	155	1.2	0.8
	100	12	203	2.03	65	1.0	0.7
CLEVIOS™ P VP CH 8000	50	7	179	3.58	61	1.7	1.2
	100	7	355	3.55	14	1.4	1.2

(a) time to reach a luminance of 100 cd/m^2.

Taking into account the EL spectrum (Figure S15), we calculated the corresponding power conversion efficiency (PCE) and external quantum efficiency (EQE). We obtained maximum PCE close to 1 lm W−1, while the EQE peaks at 0.7−0.8%, being slightly higher for the LECs biased at 50 cd m^{-2}. LECs prepared on the PSS-rich CLEVIOS™ P VP CH 8000 show a distinctive behavior. Independent of the current density used, the LECs turn on immediately after biasing (t_{on} < 7 s) to reach brightness levels much higher than those obtained with the other PEDOT:PSS formulation (Figure 6c). In particular, we measured L_{max} of 179 and 355 cd m^{-2}, corresponding to efficacies of 3.58 and 3.55 cd A^{-1} for LECs driven at 50 and 100 A m^{-2},

respectively. These values are among the highest reported for LECs employing $[Cu(P^P)(N^N)]^+$ complexes as emitters.[9,10,11,12,13] As the increased luminescence is accompanied by only a small increase in the voltage, we obtained PCE_{max} of 1.7 and 1.4 lm W^{-1} for the high and low current density driven devices, respectively. Importantly, the maximum EQE is current density-independent and was found to be 1.2%, which is remarkable for this type of iTMCs. As often seen in LECs, higher current densities lead to more intense emission but at the expense of stability.[29] The brightest devices (driven at 100 A m^{-2}) exhibit a fast electroluminescence decay, with $t_{1/2}$ = 14 minutes. The lifetime of LECs driven at lower current density is of about 1 hour, but the luminance is still at 50 cd m^{-2} after 3 hours of operation.

In order to shed light on the possible origin of the different device performance observed using different PEDOT:PSS formulation, we evaluated the photoluminescence of [Cu(BnN-xantphos)(Me_2bpy)][PF_6] on several substrates. We prepared thin films of the complex in the presence of the ionic liquid [EMIM][PF_6] to mimic the emissive layer composition, using quartz, and quartz coated with CLEVIOS™ P VP AI 4083 or CLEVIOS™ P VP CH 8000. The PLQY of the film on quartz is 17% (with excitation at 360 nm), which is lower than the value recorded in powder (55%), a behavior often observed for this type of copper(I) complexes. Interestingly, the PLQY was found to decrease substantially (10%) when the complex is deposited onto CLEVIOS™ P VP AI 4083, while it is unvaried (17%) when the quartz is coated with the low conducting grade PEDOT:PSS. This observation suggests that the improved performance with the low conducting PEDOT:PSS grade is related to the decreased exciton quenching, rather than to the larger WF. The substrate-induced luminescence quenching can be due to either the larger conductivity of the CLEVIOS™ P VP AI 4083 (i.e., exciton quenching due to free-carrier in the PEDOT:PSS), or to a difference in morphology.

Hence we investigated the surface of [Cu(BnN-xantphos)(Me_2bpy)][PF_6]:[EMIM][PF_6] films deposited on the two types of PEDOT:PSS by atomic force microscopy (AFM, Figure S16). The film morphology on top of the CLEVIOS™ P VP AI 4083 is composed of round aggregates with diameter ranging from a few tens to 100 nm. The root-mean-square roughness (R_{RMS}, calculated over an area of 4 μm^2) is 10.3 nm, with a peak-to-peak roughness (R_{PTP}) as high as 85.9 nm. Interestingly, we found a substantially reduced roughness when the [Cu(BnN-xantphos)(Me_2bpy)][PF_6] films are deposited onto the CLEVIOS™ P VP CH 8000 injection layer. The R_{RMS} is only 0.2 nm, with a RPTP as low as 2.0 nm, indicating an extremely flat and homogeneous surface. As the surface roughness of bare PEDOT:PSS is rather independent on the PSS content,[28] the different morphology observed must be due to a different film-formation, driven by the chemical nature of the surface and its affinity with the Cu(I) compound. In this case, the larger ionic density of the PSS-rich CLEVIOS™ P VP CH 8000, might be beneficial for the film formation of our ionic iTMC.

4. Conclusions

We have reported the series of copper(I) complexes [Cu(HN-xantphos)(N^N)][PF_6] and [Cu(BnN-xantphos)(N^N)][PF_6] in which N^N = bpy, Mebpy and Me_2bpy. All compounds have been fully characterized in solution by multinuclear NMR spectroscopy, and the single crystal structures of [Cu(HN-xantphos)(Mebpy)][PF_6] and [Cu(BnN-xantphos)(Me_2bpy)][PF_6] confirm distorted tetrahedral copper(I) coordination geometries with N^N and P^P chelating ligands. Electrochemical and solution photophysical properties of the BnN-xantphos-containing compounds (for which the HOMO is located on the phenoxazine moiety) were investigated. The first oxidation of [Cu(BnN-xantphos)(N^N)][PF_6] is significantly lower in potential than previously reported for analogous xantphos-containing complexes.26 This is consistent with the former being BnN-

xantphos ligand-centered while the latter are metal-centered. The absorption spectra of the [Cu(BnN-xantphos)(N^N)][PF_6] compounds have been interpreted with the aid of TD-DFT calculations. The compounds are weakly emissive in solution with a blue-shift from 650 to 600 to 560 nm along the series [Cu(BnN-xantphos)(bpy)][PF_6], [Cu(BnN-xantphos)(Mebpy)][PF_6] to [Cu(BnN-xantphos)(Me_2bpy)][PF_6]. The solid-state emission behaviour of the [Cu(HN-xantphos)(N^N)][PF_6] and [Cu(BnN-xantphos)(N^N)][PF_6] compounds demonstrates blue-shifts on going from bpy to Mebpy to Me_2bpy, and a small red-shift as the benzyl group is introduced into the phenoxazine moiety of the P^P ligand.

[Cu(BnN-xantphos)(Me_2bpy)][PF_6] exhibits a solid-state PLQY of 55% with an excited state lifetime of 17.4 μs, and in view of this high PLQY, [Cu(BnN-xantphos)(Me_2bpy)][PF_6] was used as the emitting layer in light-emitting electrochemical cells. The devices exhibit promising lifetime, intense electroluminescence, and quantum efficiency exceeding 1%, among the highest reported for similar $[Cu(P^P)(N^N)]^+$ compounds. We also highlight the importance of the choice of appropriate hole injection layers, which can reduce the exciton quenching without undermining the device operation.

5. Experimental Section. Experimental details (instruments, synthesis, crystallography and computational details) are given in the supporting information.

Supporting Information

Supporting Information is available from the Wiley Online Library or from the author.

Acknowledgements

We are grateful to the University of Basel, the Spanish Ministry of Economy and Competitiveness (MINECO, MAT2017-88821-R, PGC2018-099568-B-I00, PCIN-2017-014 and Unidad de Excelencia María de Maeztu MDM-2015-0538), the Generalitat Valenciana (PROMETEO/2016/135), and European FEDER funds (PGC2018-099568-B-I00) for financial support. MS thanks the Spanish Ministry for his RyC contract.

Received: ((will be filled in by the editorial staff))
Revised: ((will be filled in by the editorial staff))
Published online: ((will be filled in by the editorial staff))

We describe the synthesis and characterization of a series of copper(I) $[Cu(P^P)(N^N)]^+$ complexes with modified bisphosphane ligands. The introduction of a peripheral N-bonded benzyl domain in the P^P ligand BnN-xantphos results in solid-state photoluminescence quantum yield of 55%. Bright LECs were obtained with $[Cu(BnN\text{-}xantphos)(Me_2bpy)][PF_6]$, and we show that the electroluminescence quantum yield can be improved by judicious choice of the hole injection layers.

Keyword ionic copper complexes, DFT, photophysics, electroluminescence, light-emitting electrochemical cells

N. Arnosti, F. Brunner, I. Susic, S. Keller, J. M. Junquera-Hernández, A. Prescimone, H. J. Bolink, M. Sessolo,* E. Ortí,* C. E. Housecroft* and E. C. Constable

Remote modification of bidentate phosphane ligands controls photonics properties in their complexes: CMe_2 to NR replacement results in enhanced performance of [Cu(RN-xantphos)(N^N)][PF_6] complexes in light-emitting electrochemical cells.

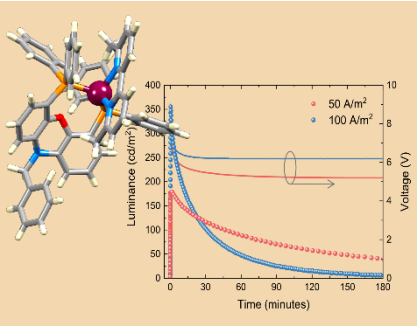

1 M.T. Buckner, D.R. McMillin, *J. Chem. Soc., Chem. Commun.* **1978**, 759.
2 R.A. Rader, D.R. McMillin, M.T. Buckner, T.G. Matthews, D.J. Casadonte, R.K. Lengel, S.B. Whittaker, L.M. Darmon, F.E. Lytle, *J. Am. Chem. Soc.* **1981**, *103*, 5906.
3 R.D. Costa, E. Ortí, H.J. Bolink, F. Monti, G. Accorsi, N. Armaroli, *Angew. Chem. Int. Ed*. **2012**, *51*, 8178.
4 M. Elie, S. Gaillard, J.-L. Renaud in *Light-emitting electrochemical cells: concepts, advances and challenges*, (Ed. R.D. Costa), Springer, Cham, 2017, Ch. 11, p. 287.
5 E. Fresta, R.D. Costa, *J. Mater. Chem. C* **2017**, *5*, 5643.
6 M.J. Leitl, V.A. Krylova, P.I Djurovich, M.E. Thompson, H. Yersin, *J. Am. Chem. Soc.* **2014**, *136*, 16032.
7 H. Yersin, R. Czerwieniec, M.Z. Shafikov, A.F. Suleymanova, *ChemPhysChem* **2017**, *18*, 3508.
8 R. Czerwieniec, M.J. Leitl, H.H.H. Homeier, H. Yersin, *Coord. Chem. Rev.* **2016**, *325*, 2 and references therein.
9 S. Keller, E.C. Constable, C.E. Housecroft, M. Neuburger, A. Prescimone, G. Longo, A. Pertegás, M. Sessolo, H.J. Bolink, *Dalton Trans.* **2014**, *43*, 16593.
10 S. Keller, A. Pertegás, G. Longo, L. Martinez, J. Cerdá, J.M. Junquera-Hernández, A. Prescimone, E.C. Constable, C.E. Housecroft, E. Ortí, H.J. Bolink, *J. Mater. Chem. C* **2016**, *4*, 3857.
11 M. Alkan-Zambada, S. Keller, L. Martínez-Sarti, A. Prescimone, J.M. Junquera-Hernández, E.C. Constable, H.J. Bolink, M. Sessolo, E. Ortí, C.E. Housecroft, *J. Mater. Chem. C* **2018**, *6*, 8460.
12 E. Fresta, G. Volpi, M. Milanesio, C. Garino, C. Barolo, R.D. Costa, *Inorg. Chem.* **2018**, *57*, 10469.
13 R.D. Costa, Ed. *Light-emitting electrochemical cells: concepts, advances and challenges*, Springer, Cham, 2017.
14 See for example: C. Hierlinger, E. Trzop, L. Toupet, J. Ávila, M.-G. La-Placa, H.J. Bolink, V. Guerchais, E. Zysman-Colman, *J. Mater. Chem. C* **2018**, *6*, 6385.
15 S. Keller, A. Prescimone, E.C. Constable, C.E. Housecroft, *Photochem. Photobiol. Sci.* **2018**, *17*, 375.
16 L.A. van der Veen, P.H. Keeven, G.C. Schoemaker, J.N.H. Reek, P.C.J. Kamer, P.W.N.M. van Leeuwen, M. Lutz, A.L. Spek, *Organometallics* **2000**, *19*, 872.
17 R.P.J. Bronger, P.C.J. Kamer, P.W.N.M. van Leeuwen, *Organometallics* **2003**, *22*, 5358.
18 J. Zhang, A. Bellomo, N. Trongsiriwat, T. Jia, P.J. Carroll, S.D. Dreher, M.T. Tudge, H. Yin, J.R. Robinson, E.J. Schelter, P.J. Walsh, *J. Am. Chem. Soc.* **2014**, *136*, 6276.
19 L. Ping, D.S. Chung, J. Bouffard, S. Lee, *Chem. Soc. Rev.* **2017**, *46*, 4299.
20 See for example: H. Juang, S.-C. Sha, S.A. Jeong, B.C. Manor, P. J. Walsh, *Org. Lett.* **2019**, *21*, 1735; D. Pingen, J.-H. Choi, H. Allen, G. Murray, P. Ganji, P.W.N.M. van Leeuwen, M.H.G. Prechtl, D. Vogt, *Catal. Sci. Technol.* **2018**, *8*, 3969; J. Mao, J. Zhang, S. Zhang, P.J. Walsh, *Dalton Trans.* **2018**, *47*, 8690 and references therein.
21 S.-P. Luo, E. Mej, A. Friedrich, A. Pazidis, H. Junge, A.-E. Surkus, R. Jackstell, S. Denurra, S. Gladiali, S. Lochbrunner, M. Beller, *Angew. Chem. Int. Ed.* **2013**, *52*, 419.
22 C.P. Casey, G.T. Whiteker, *Isr. J. Chem.* 1990, *30*, 299.
23 F. Brunner, S. Graber, Y. Baumgartner, D. Häussinger, A. Prescimone, E. C. Constable, C. E. Housecroft, *Dalton Trans.* **2017**, *46*, 6379.
24 M. Nishio, CrystEngComm **2004**, *6*, 130; M. Nishio, Y. Umezawa, K. Honda, S. Tsuboyama, H. Suezama, *CrystEngComm* **2009**, *11*, 1757.

25 S. Keller, A. Prescimone, H.J. Bolink, M. Sessolo, G. Longo, L. Martínez-Sartí, J.M. Junquera-Hernández, E.C. Constable, E. Ortí, C.E. Housecroft, *Dalton Trans*. **2018**, *47*, 14263-14276
26 S. Keller, F. Brunner, J.M. Junquera-Hernández, A. Pertegás, M.-G. La-Placa, A. Prescimone, E.C. Constable, H.J. Bolink, E. Ortí, C.E. Housecroft, *ChemPlusChem* 2018, *83*, 217.
27 F. Brunner, A. Babaei, A. Pertegás, J.M. Junquera-Hernández, A. Prescimone, E.C. Constable, H.J. Bolink, M. Sessolo, E. Ortí, C.E. Housecroft, *Dalton Trans*. **2019**, *48*, 446.
28 A. Elschner, S. Kirchmeyer, W. Lovenich, U. Merker, K. Reuter, *PEDOT: Principles and Applications of an Intrinsically Conductive Polymer*, 2010, CRC Press, Boca Raton.
29 A.M. Bünzli, E.C. Constable, C.E. Housecroft, A. Prescimone, J.A. Zampese, G. Longo, L. Gil-Escrig, A. Pertegás, H.J. Bolink, *Chem. Sci.* **2015**, *6*, 2843.